eLIFE elifesciences.org

RESEARCH ARTICLE

Figures and figure supplements

A prediction model of working memory across health and psychiatric disease using whole-brain functional connectivity

Masahiro Yamashita *et al*

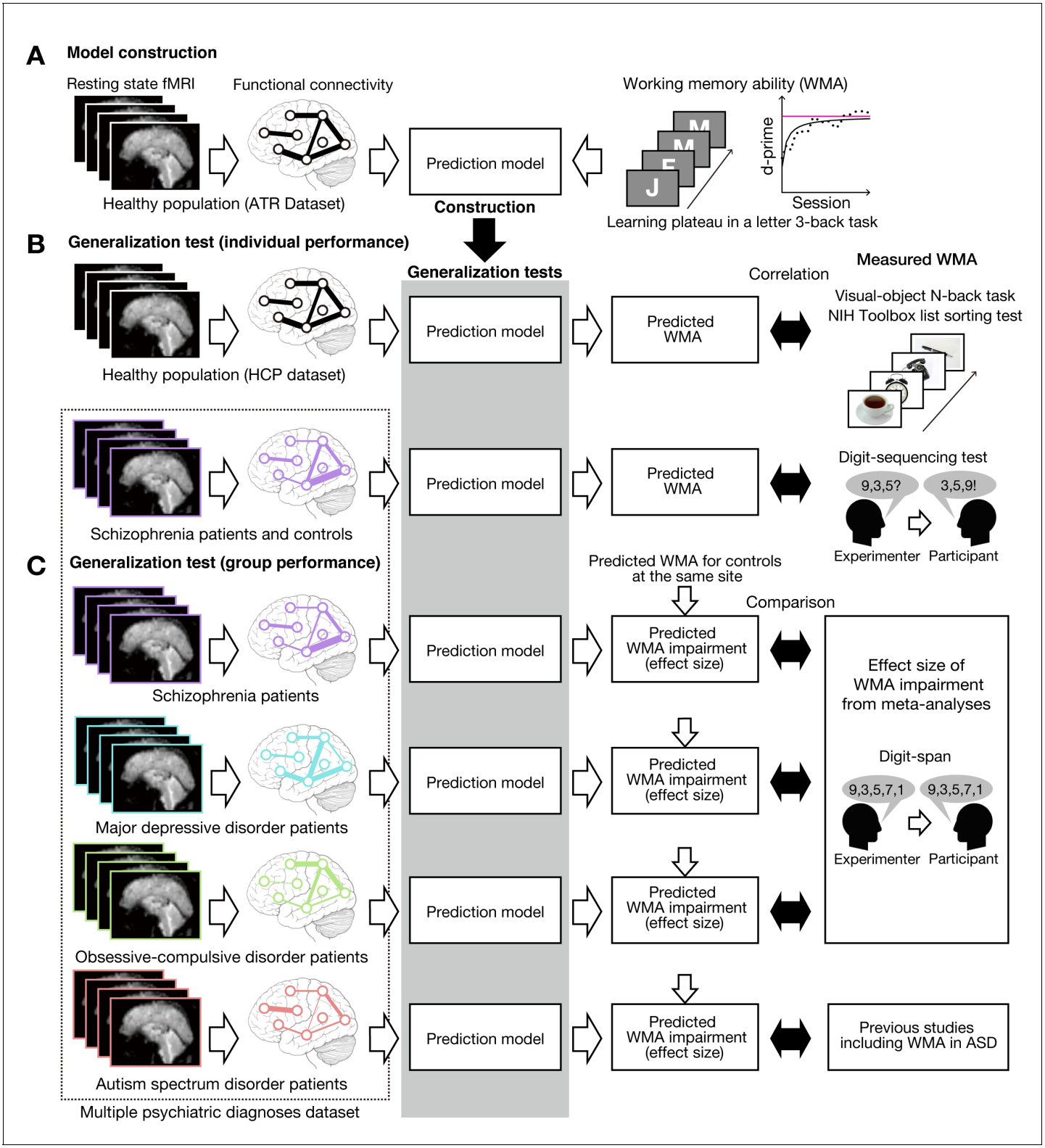

Figure 1. Schematic diagram of model construction and generalization tests using independent datasets. (**A**) Model was developed using a whole-brain resting state FC and a learning plateau of a letter 3-back task within healthy individuals from ATR dataset. (**B**) We applied the model to resting state FC patterns and predicted individual participant's working memory ability. We first examined the external validity using an independent USA healthy dataset (HCP dataset: the upper flow chart in (**B**)). The predicted working memory ability was compared to actual working memory performance (visual-object N-back task and the NIH toolbox list sorting test). Then we examined the generalizability to a clinical population using a schizophrenia

Figure 1 continued on next page

Figure 1 continued

dataset (the lower flow chart in (**B**)). The predicted working memory ability was compared to actual working memory score measured by Digit sequencing test. (**C**) Using the multiple psychiatric diagnoses dataset, degree of working memory impairment for each diagnosis was predicted as differences from corresponding controls. The predicted impairments were validated by previous meta-analysis studies on digit-span across multiple diagnoses. Note that the HCP dataset's task stimuli images are just illustration purpose and different from the original stimuli.

DOI: https://doi.org/10.7554/eLife.38844.002

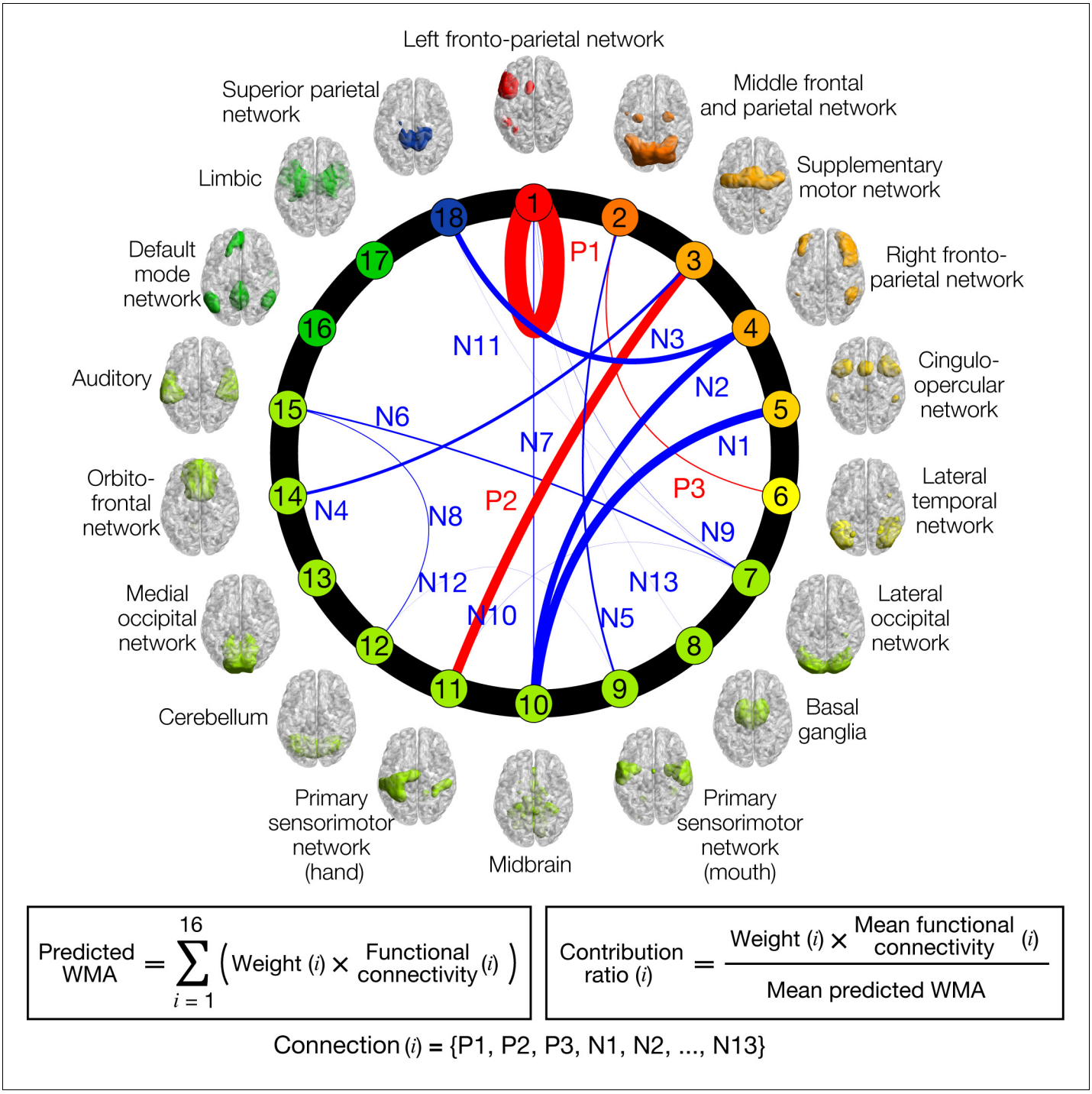

Figure 2. Normative model of working memory ability (WMA). Circle plot of networks and their connections in the model. Individual letter 3-back learning plateaus are predicted by a linear weighted summation of 16 FC values at 16 connections selected by a sparse linear regression algorithm. Connection thicknesses indicate contribution ratios (weight x FC at each connection). Connections are labeled 'Positive/Negative (P/N)' based on correlation coefficient signs with letter 3-back learning performances, whereas numbers indicate descending orders of contribution ratio. Each network's color indicates relevance with working memory function based on BrainMap ICA (***Laird et al., 2011***); warmer colors indicate closer relevance to working memory function. See ***Table 1*** for the networks connected by the selected 16 connections, and precise values of contribution ratio of each connection. Each network's label and regions included in it are summarized in ***Supplementary file 2***.

DOI: https://doi.org/10.7554/eLife.38844.003

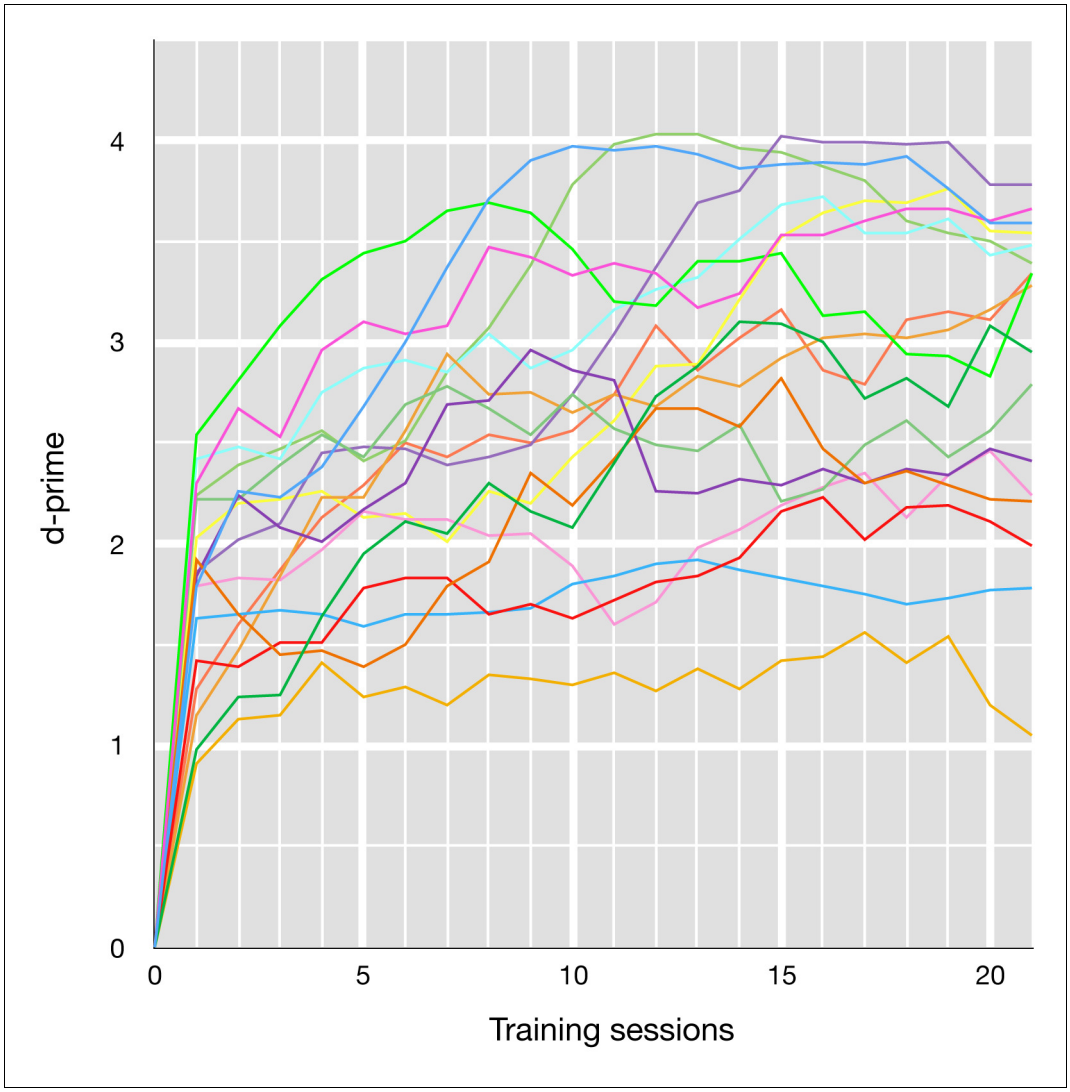

Figure 2—figure supplement 1. Letter 3-back learning curves for each participant. Data points were five-session moving averaged (e.g. training session one plots average d-prime from sessions 1 to 5).
DOI: https://doi.org/10.7554/eLife.38844.004

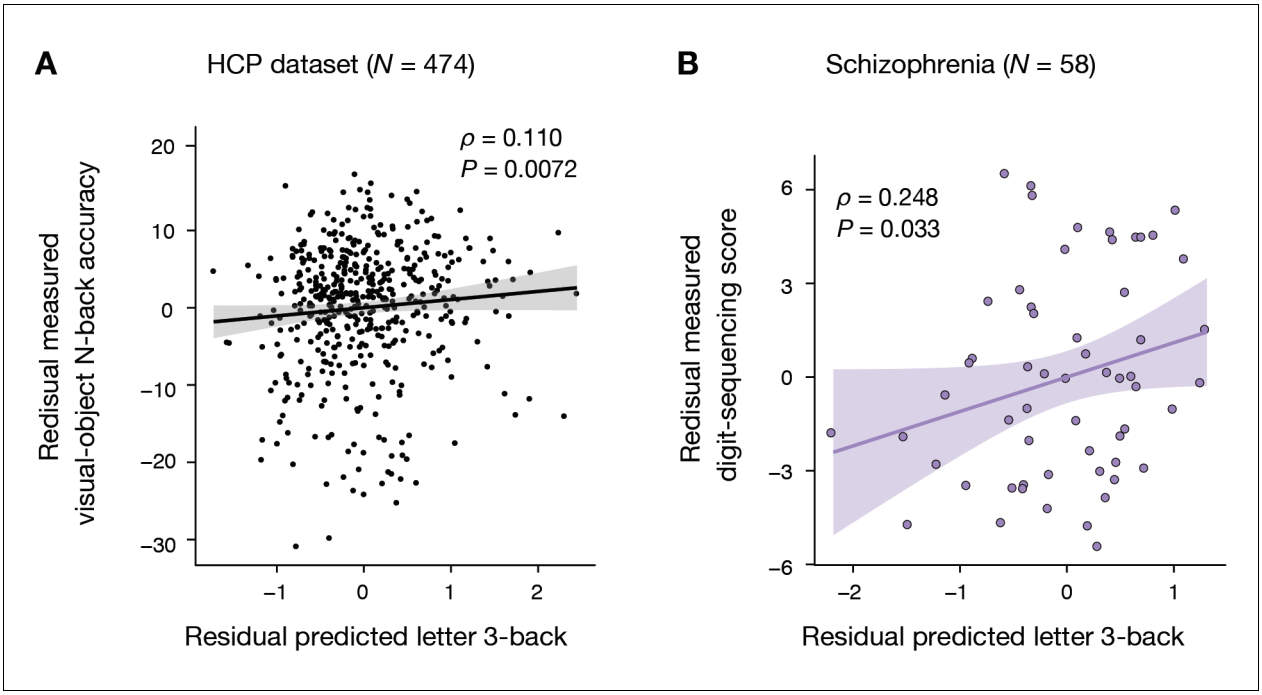

Figure 3. Generalizability to HCP dataset and schizophrenia dataset. (**A**) Significant Spearman's rank partial correlation between predicted letter 3-back learning performance and measured visual-object N-back accuracy while factoring out general fluid intelligence and head motion (ρ = 0.110, p = 0.0072). (**B**) Significant Pearson partial correlation between predicted letter 3-back performances and measured digit-sequencing scores while factoring out the composite BACS score and age (ρ = 0.248, p = 0.033).

DOI: https://doi.org/10.7554/eLife.38844.005

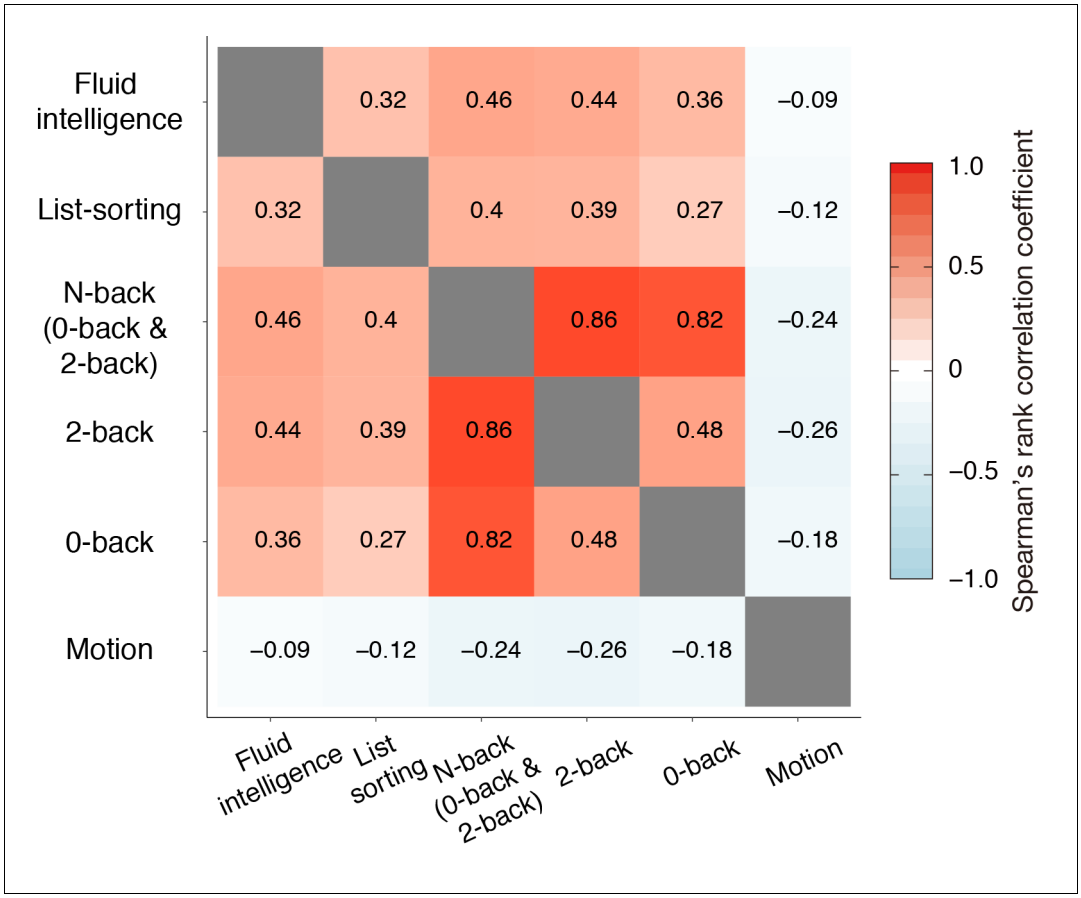

Figure 3—figure supplement 1. Spearman's rank correlation matrix for HCP dataset.
DOI: https://doi.org/10.7554/eLife.38844.006

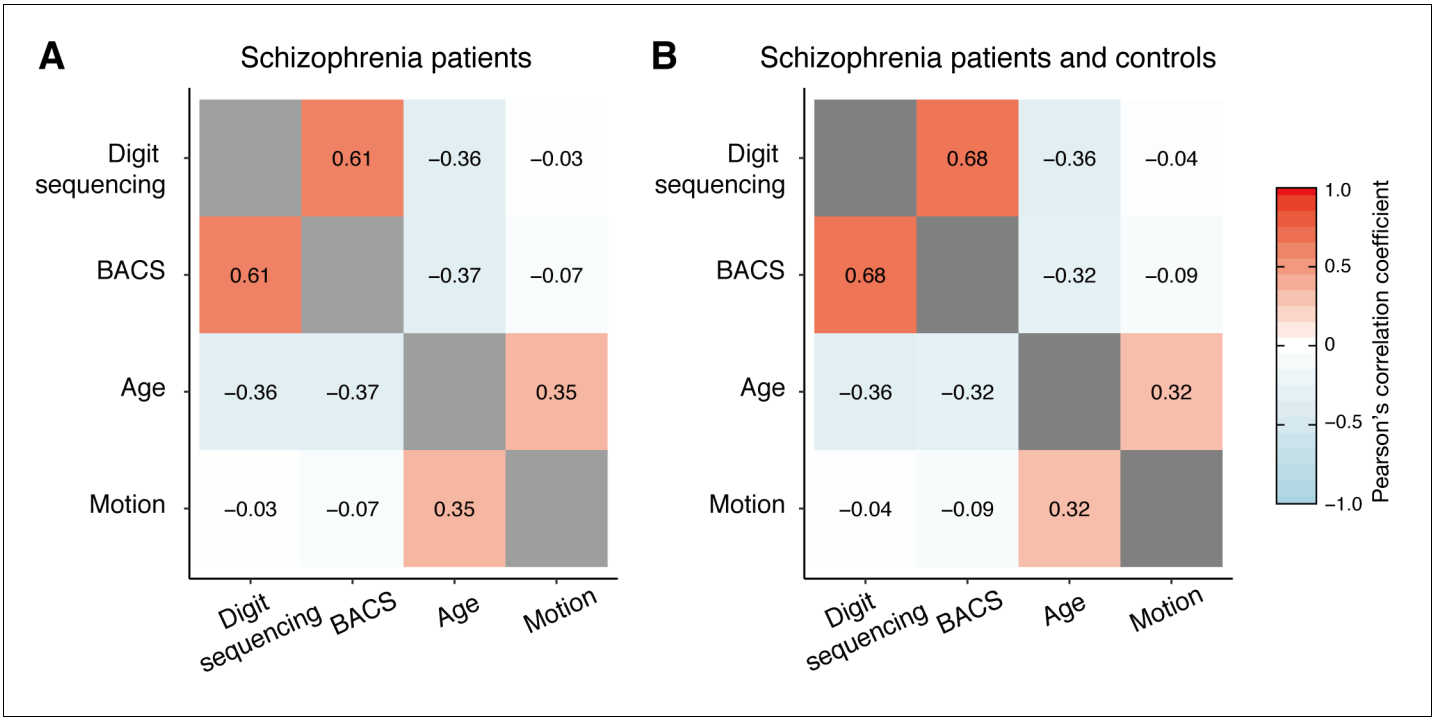

Figure 3—figure supplement 2. Pearson's correlation matrices for schizophrenia samples. (**A**) Correlation among schizophrenia patients (N = 58). (**B**) Correlation among schizophrenia patients and controls (N = 118).

DOI: https://doi.org/10.7554/eLife.38844.007

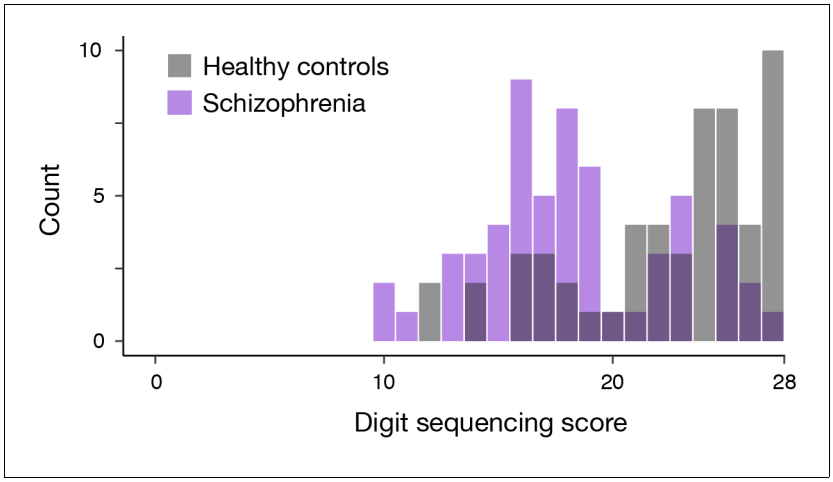

Figure 3—figure supplement 3. Distribution of BACS digit-sequencing score. The count of healthy controls increased toward the maximum score (28), and the largest count was found for the maximum score. This suggests a ceiling effect in the healthy controls.

DOI: https://doi.org/10.7554/eLife.38844.008

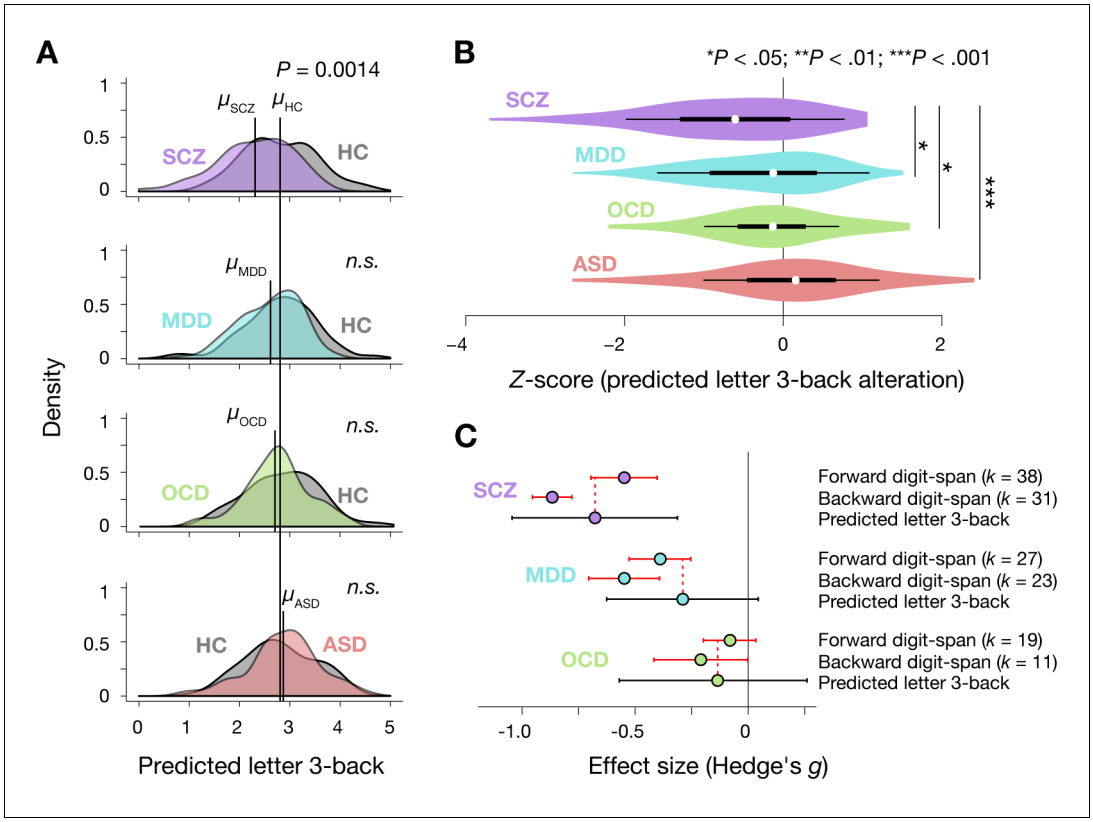

Figure 4. Prediction of diagnosis-specific alterations of working memory ability. (**A**) Predicted letter 3-back working memory ability for patients (*N* = 58, 77, 45, and 69 for SCZ, MDD, OCD, and ASD, respectively) and their age- and gender-matched healthy/typically developed controls (HC, *N* = 60, 62, 47, and 71) shown as kernel density. For illustration purposes, distribution of each control group was standardized to that of the ATR dataset, and the same linear transformation was applied to patients' distributions. μ indicates mean value for each group. (**B**) Violin plots of *Z*-scores for predicted working memory ability alterations. White circles indicate medians. Box limits indicate 25th and 75th percentiles. Whiskers extend 1.5 times interquartile range from 25th and 75th percentiles. (**C**) Comparison of estimated effect sizes for working memory deficits. *k* indicates number of studies included in the meta-analyses (***Forbes et al., 2009***; ***Snyder, 2014***; ***Snyder et al., 2015***). Error bars indicate 95% confidence intervals.

DOI: https://doi.org/10.7554/eLife.38844.009

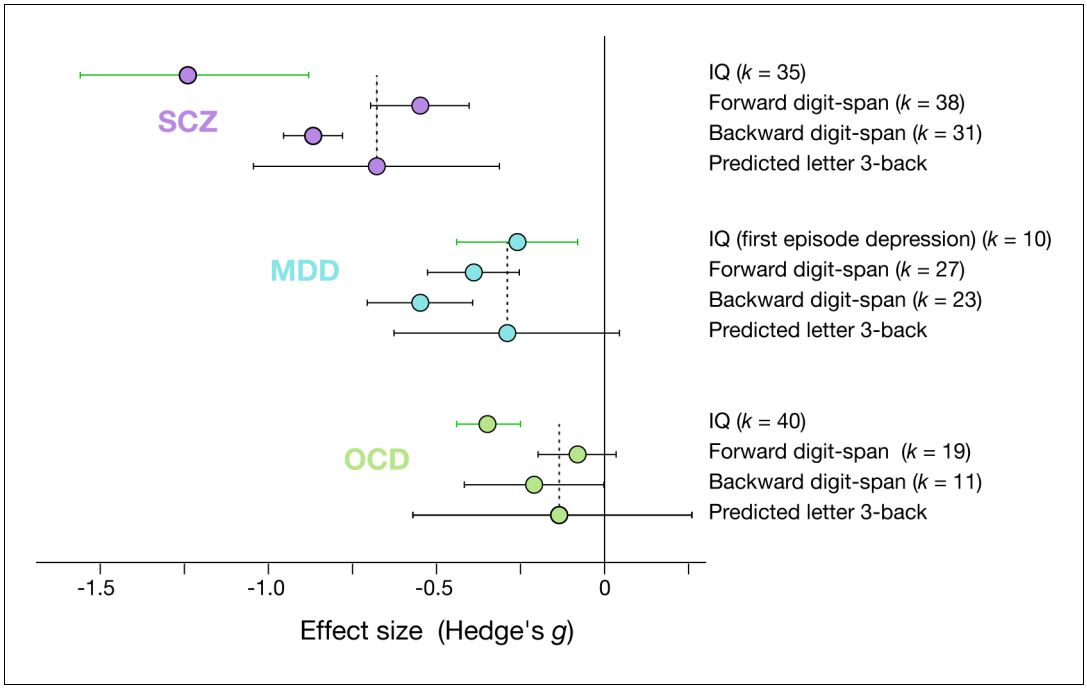

Figure 4—figure supplement 1. Effect sizes of IQ, digit-span, and predicted working memory ability. *k* indicates number of studies included in the meta-analyses (***Abramovitch et al., 2018***; ***Ahern and Semkovska, 2017***; ***Heinrichs and Zakzanis, 1998***). Error bars indicate 95% confidence intervals.

DOI: https://doi.org/10.7554/eLife.38844.010

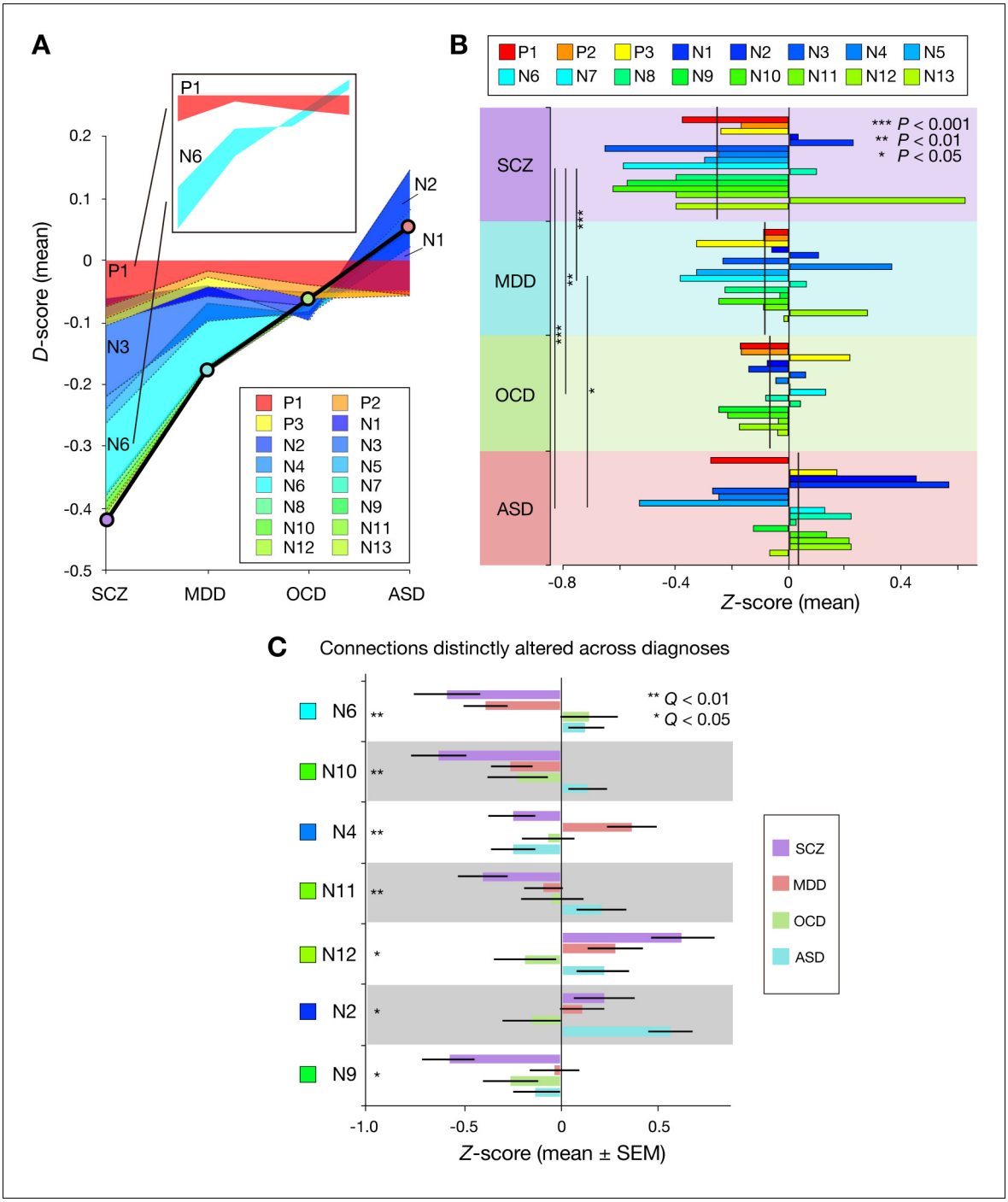

Figure 5. Accumulation of function connectivity differences exhibits diagnosis-specific working memory ability. (**A**) Accumulation of averaged *D*-scores for all 16 connections. Bold black line indicates summation of contributions by all connections, corresponding to predicted working memory ability alteration. This figure shows how diagnosis-specific working memory impairment results from complex disturbances of multiple connections. Upper panel depicts two representative alteration patterns across diagnoses. While connection P1 commonly decreased working memory ability across diagnoses, connection N6 distinctly affected working memory ability (decrease in SCZ and MDD and increase in OCD and ASD). (**B**) *Z*-scores (normalized *D*-scores) for each diagnosis. Left asterisks and lines indicate significant differences in mean *Z*-scores between two diagnoses ($p < 0.05$, Bonferroni corrected). Vertical lines across horizontal bars indicate *Z*-scores averaged across connections. (**C**) *Z*-scores for connection that showed a significant effect of diagnosis. Connections were sorted by small p values of diagnosis effect (Kruskal-Wallis test, $Q < 0.05$, FDR corrected).

DOI: https://doi.org/10.7554/eLife.38844.013

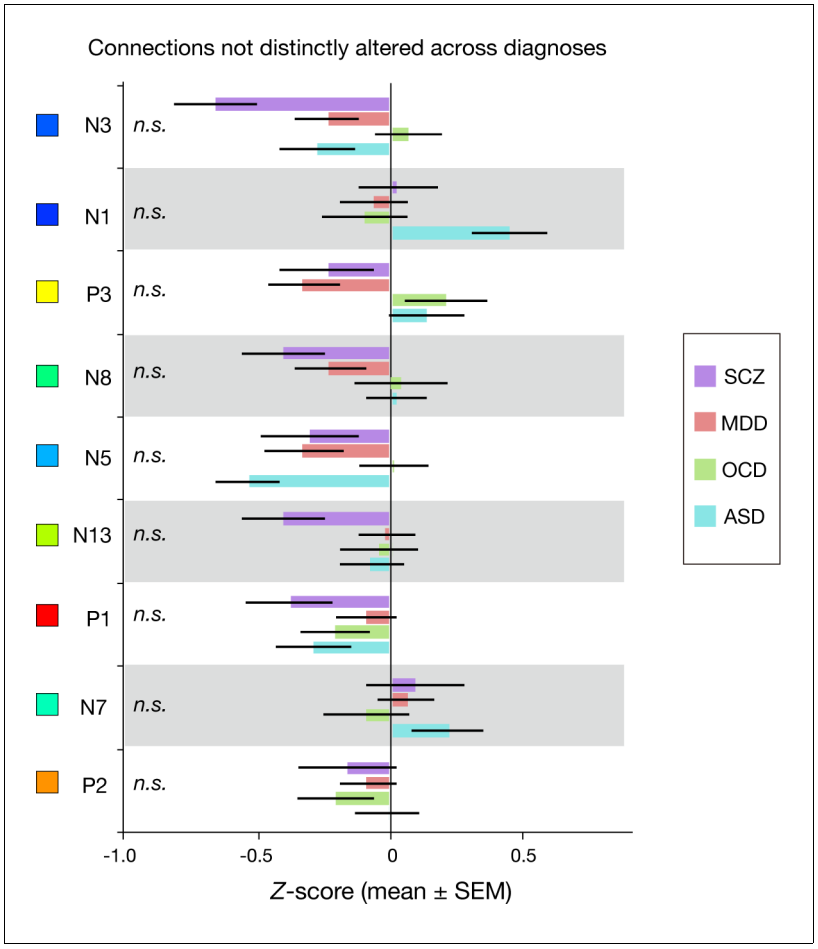

Figure 5—figure supplement 1. Connections of non-significant effect of diagnosis.
DOI: https://doi.org/10.7554/eLife.38844.014

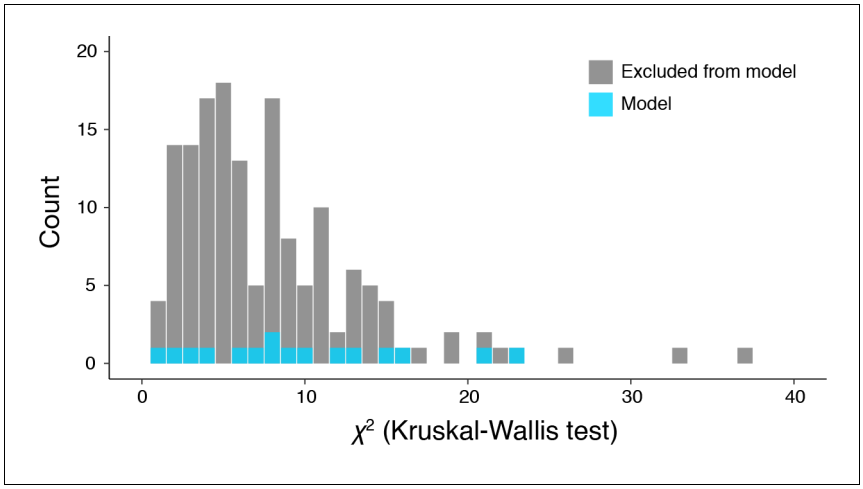

Figure 5—figure supplement 2. Distribution of magnitude of diagnosis effect on connectivity change between the connections in the model and other connections. The horizontal axis shows chi-square values of a Kruskal-Wallis test for each connection. There was no significant difference between the two groups (two-sample Kolmogorov-Smirnov test, p = 0.30).

DOI: https://doi.org/10.7554/eLife.38844.015

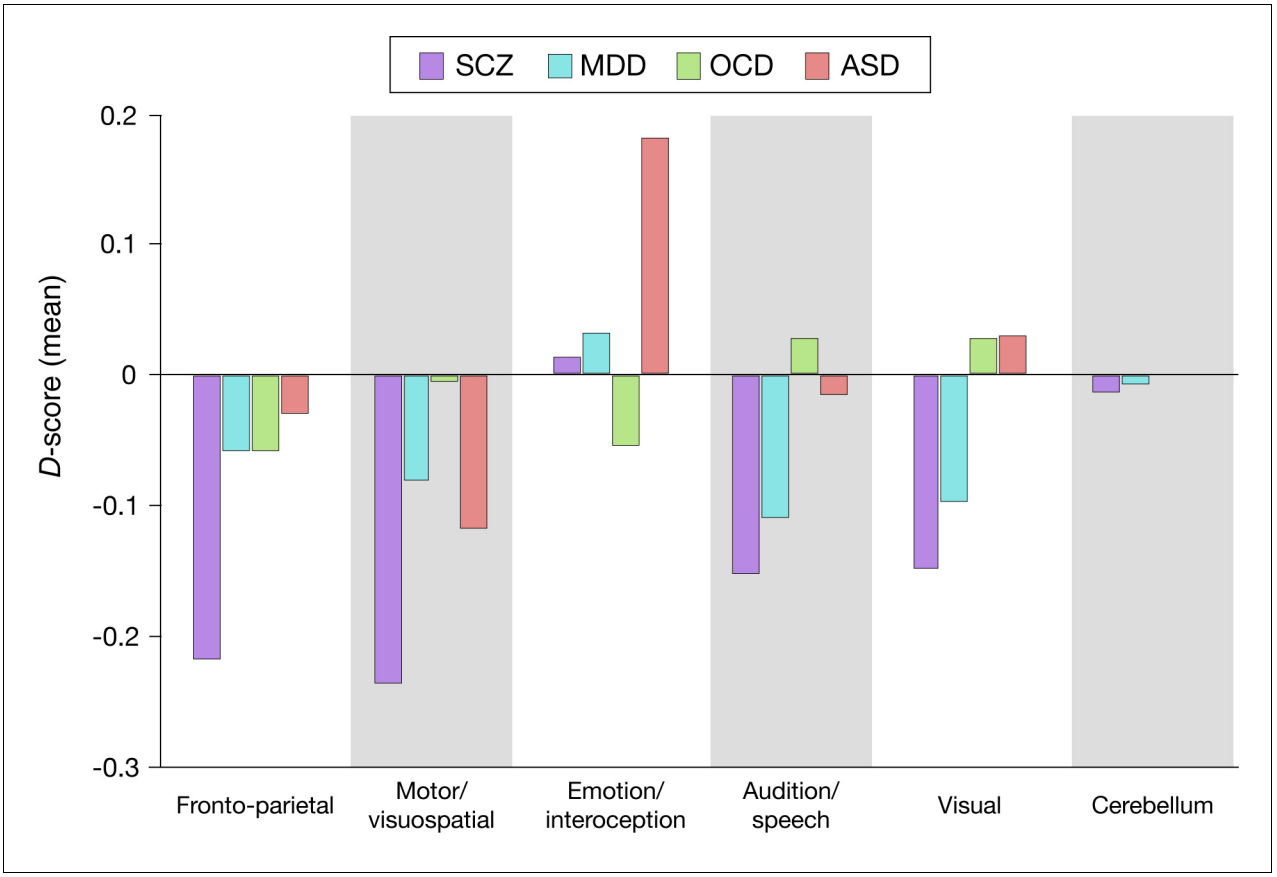

Figure 5—figure supplement 3. *D*-scores related to network clusters.
DOI: https://doi.org/10.7554/eLife.38844.016